For values of α greater than α_{cr}, the two roots of Eq. (25) are complex, indicating escape (no potential well), as shown in the lowest curve in Fig. 2.

Shifted Circular Orbits

The local minimum points of the upper two potential energy curves in Fig. 2 represent the locations of stable circular orbits at radii larger than r_0. This is because an outward radial thrust acceleration has the effect of decreasing the value of the local gravitational acceleration. An inward radial thrust ($\alpha < 0$) increases the effective value of the gravitational acceleration, resulting in a stable circular orbit at a radius less than r_0. The upper two curves in Fig. 2 both exhibit a single local minimum at a value of $r > r_0$. The lowest curve is the limiting case, where the local minimum ceases to exist.

For a circular orbit of radius r_c, the orbital speed is $v_c = r_c\dot{\theta}_c$ and $\dot{r}_c = \ddot{r}_c = 0$. Equation (3) then yields

$$v_c^2 = (\mu/r_c) - a_r r_c \tag{26}$$

The shifted circular orbit period in the presence of the radial thrust can then be determined simply as

$$P = \frac{2\pi r_c}{v_c} = 2\pi\left[\frac{r_c^3}{\mu}\right]^{\frac{1}{2}} \frac{1}{\left[1 - \left(a_r r_c^2/\mu\right)\right]^{\frac{1}{2}}}$$

$$= \frac{P_c}{\left[1 - \left(a_r r_c^2/\mu\right)\right]^{\frac{1}{2}}} = \frac{P_c}{\left[1 - \alpha(r_c/r_0)^2\right]^{\frac{1}{2}}} \tag{27}$$

where P_c is the no-thrust circular orbit period at radius r_c.

From Eq. (27) it is evident that $P > P_c$ if $\alpha > 0$ and $P < P_c$ if $\alpha < 0$. This means that for $\alpha > 0$ a shifted circular orbit of period P will have a radius smaller than the no-thrust circular orbit with the same period. As a specific example of a shifted orbit, consider a geosynchronous orbit. Take the maximum-shift value of $\alpha = \frac{4}{27} = 0.148148$ corresponding to a shifted circular orbit at $r_c = 1.5r_0$. (This orbit is actually unstable, and so a slightly smaller value of α would need to be used in practice.) For $P = 23.934$ h, Eq. (25) yields a value of $P_c = 19.542$ h, corresponding to a shifted circular orbit of radius of 36,834 km. This is 5330 km lower than the conventional (no-thrust) geosynchronous radius of 42,164 km, but the period is the same. In terms of orbital altitude, this represents a 15% decrease. The level of constant radial thrust acceleration necessary to maintain this orbit is about 0.1 m/s^2 or approximately 10^{-2} g. This lower altitude geosynchronous orbit may provide some advantages. A shifted 1-year heliocentric orbit requires a much lower thrust acceleration of 0.0026 m/s^2.

Conclusions

The use of constant radial thrust acceleration on a circular orbit in the two-body problem is revisited. The concept of a potential energy well provides an explanation of why a radial oscillation occurs for values of thrust acceleration below a critical value and escape occurs for higher thrust levels. This critical value of thrust acceleration is determined, along with a formula for the value of the radius at which escape energy is achieved and a formula for the amplitude of the radial oscillation if escape does not occur. The concept of using a constant radial thrust acceleration to shift the radius of a circular orbit of specified period (or shift the period for a specified radius) is shown to be feasible and potentially useful for Earth-orbit and heliocentric applications.

References

[1]Tsien, H. S., "Take-Off from Satellite Orbit," *Journal of the American Rocket Society*, Vol. 23, No. 4, 1953, pp. 233–236.

[2]Battin, R. H., *An Introduction to the Mathematics and Methods of Astrodynamics*, AIAA Education Series, AIAA, New York, 1987, pp. 408–415.

[3]Boltz, F. W., "Orbital Motion Under Continuous Radial Thrust," *Journal of Guidance, Control, and Dynamics*, Vol. 14, No. 3, 1991, pp. 667–670.

[4]Boltz, F. W., "Orbital Motion Under Continuous Tangential Thrust," *Journal of Guidance, Control, and Dynamics*, Vol. 15, No. 6, 1992, pp. 1503–1507.

Two-Degree-of-Freedom $\mathcal{H}_\infty$ Robust Controller for a Flexible Missile

K. Koshy George* and M. Seetharama Bhat†
Indian Institute of Science, Bangalore 560 012, India

Introduction

THE introduction of long, slender missiles, such as the Vanguard, the Redstone, etc., has resulted in a rather acute problem of structural flexibility. These missiles are made as light as possible due to the limited thrust available, and hence structural rigidity is sacrificed. The satisfactory performance of control systems is crucially dependent on an accurate representation of the vehicle's elastic deformation under prescribed forces. This is because under adverse conditions, the control system can reinforce the amplitudes of the local elastic distortions, possibly leading to the structural failure of the vehicle. The Lark missile, built in the United States, and the ASLV-D2 launch vehicle, built by the Indian Space Research Organization, are examples of vehicles that exhibited such a control and structure interaction. Therefore, it is important that the effect of structural flexibility be directly controlled. However, because there is uncertainty in the representation of the elastic modes, robust controllers are to be designed.

We design an $\mathcal{H}_\infty$ robust two-degree-of-freedom (DOF) robust pitch plane flight control system for a flexible missile. The cascade compensator $F(s)$ is designed using a multicriteria vector optimization technique based on the minimization of the Kreisselmeier function,[1] and the feedback compensator $K(s)$ is designed using the $\mathcal{H}_\infty$ design algorithm given by Glover and Doyle.[2] The compensator $K(s)$ is placed in the feedback path to simplify the computation of the controller.[3] A two-DOF structure is chosen to improve the time-domain performance of the closed-loop system. The design is presented in the next section.

Controlling the Pitch Plane Dynamics

The flexible missile considered is a long, slender, ballistic missile. The missile is roll stabilized a priori, and hence only the pitch plane dynamics is considered. The linearized equations of the dynamics is described in terms of the pitch angle θ, the pitch angle rate q, and the angle of attack α. The effect of flexibility is described in terms of the generalized coordinates q_j. For the example considered, data for the first three bending modes are available, and satisfy $\ddot{q}_j + 2\zeta_j\dot{q}_j\omega_j + \omega_j^2 q_j = Q_j/M_j$, $1 \le j \le 3$, where ζ_j, ω_j, Q_j, and M_j are, respectively, the damping ratio, the natural frequency, the generalized force, and the generalized mass associated with the jth bending mode. The natural frequencies are 33.94, 90.73, and 163.44 rad/s with respective damping ratios 0.00646, 0.00426, and 0.00404. We assume a second-order actuator model.

We define the plant state vector as

$$\boldsymbol{x}_p = (\theta \quad q \quad \alpha \quad \delta \quad \dot{\delta} \quad q_1 \quad \dot{q}_1 \quad q_2 \quad \dot{q}_2 \quad q_3 \quad \dot{q}_3)^T$$

where δ and $\dot{\delta}$ are the states associated with the actuator. Thus, the plant model can be represented by $y_p(s) = P(s)u_p(s)$, where u_p is the control input, and $y_p = (\theta_m \quad q_m)^T$, the measured pitch angle and pitch rate, are given by

$$\theta_m = \theta + \sum_{j=1}^{3} \phi'_{\mathrm{pg}_j} q_j, \qquad q_m = q + \sum_{j=1}^{3} \phi'_{\mathrm{rg}_j} \dot{q}_j$$

Received Oct. 31, 1997; revision received Jan. 13, 1998; accepted for publication Jan. 13, 1998.

*Research Scholar, Department of Aerospace Engineering; currently Postdoctoral Fellow, Automatic Control Research Center, Seoul National University, Seoul 151-742, Republic of Korea.

†Associate Professor, Department of Aerospace Engineering. E-mail: msbdcl@aero.iisc.ernet.in.

where ϕ'_{pg_j} and ϕ'_{rg_j} are the local slopes of the mode shape functions of the jth bending mode at the sensor locations. It is apparent that the order of the state-space model is 11, and the measurements y_p is composed of signals representing both rigid-body motions and local elastic distortions. Therefore, under certain adverse conditions, the controller can reinforce the amplitudes of these elastic deformations, possibly leading to the structural failure of the vehicle. The poles of the plant are $-0.6596 \pm i163.44$, $-0.3864 \pm i90.733$, $-0.2195 \pm i33.939$, $-32.4 \pm i0.2$, -2.8662, 2.5267, and 0.009425. The plant clearly is aerodynamically unstable.

The objectives of this design study are twofold: 1) to stabilize the aerodynamically unstable missile and 2) to provide robustness against unmodeled dynamics in general, and, in particular, to that due to the flexibility of the missile. The primary requirement of the controller is to restrict the values of the angle of attack to low values. Moreover, the peak overshoot of the response to a 1-deg step θ_m input is to be at most 10%. Further, the rise time is to be minimized, and the phase margin at the first crossover frequency and the gain margins at the three bending modes are to be maximized.

To achieve these objectives, a controller is chosen such that the $\mathcal{H}_\infty$ norm of a mixed sensitivity and complementary sensitivity performance criterion is minimized. This controller is placed in the feedback path to simplify its numerical computation.[3] Albeit a one DOF is able to achieve the robustness properties, it is observed[3] that the time-domain performance is rather unsatisfactory for this example. To overcome this problem, we insert a cascade compensator $F(s)$, and choose its parameters appropriately. A feedback compensator $K(s)$ is then synthesized via the $\mathcal{H}_\infty$ algorithm. The structure of the generalized plant is shown in Fig. 1. Clearly, this is an example of a two-DOF controller.[4] Moreover, the addition of $F(s)$ shapes the singular values of the plant model $P(s)$.

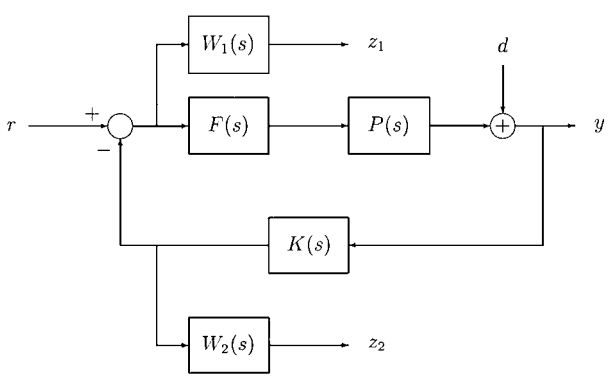

Fig. 1 Two-DOF configuration.

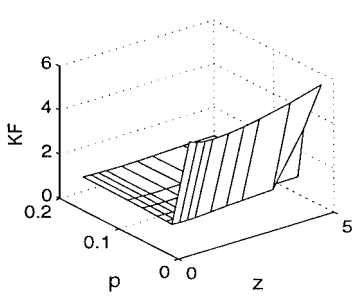

Fig. 2a Kreisselmeier function.

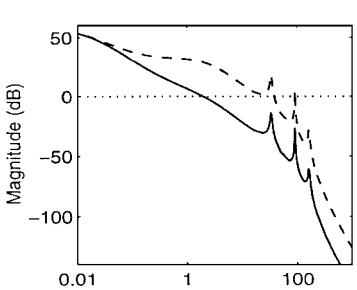

Fig. 2b Plant dynamics: – – –, unshaped, and ——, shaped.

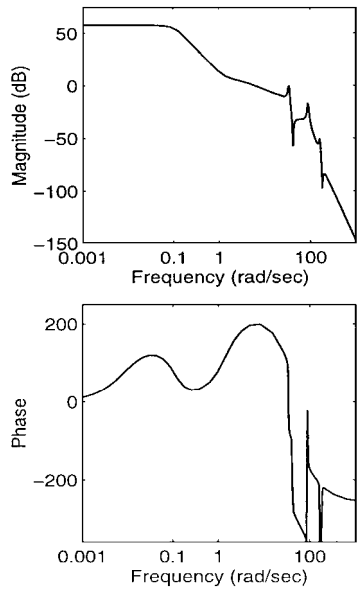

Fig. 2c Bode plot of the open-loop transfer function.

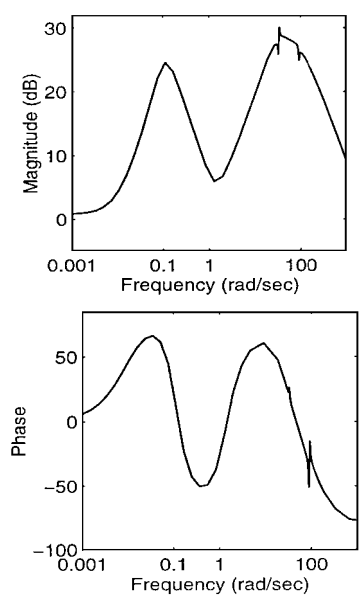

Fig. 2d Bode plot of the controller transfer function.

We choose the following structure for $F(s)$: $F(s) = p(s+z)/z(s+p) = \tilde{\tau}_1 s + 1/\tilde{\tau}_2 s + 1$. A multicriteria vector optimization technique based on the minimization of the Kreisselmeier function is applied to obtain the time constants of $F(s)$. We minimize the rise time and the peak overshoot and maximize the bandwidth, the gain and phase margins at the low crossover frequency, and the gain margins at the three modes. The technique developed by Kreisselmeier and Steinhauser[1] permits the designer to introduce these performance objectives explicitly. We apply this method to systematically choose $\tilde{\tau}_1$ and $\tilde{\tau}_2$, the parameters of $F(s)$, and, hence, achieve these design requirements. Moreover, the singular values of the plant is shaped with the addition of $F(s)$; we observe that the magnitude of the transfer function at the bending modes of the shaped plant $P(s)F(s)$ is considerably less than that of the given plant $P(s)$. The design objectives are first formulated as components of a performance vector and then converted into an equivalent scalar minimax problem. However, this function is not continuously differentiable everywhere with respect to the vector performance index and, hence,

may cause numerical problems.[1] To overcome this disadvantage, it is recommended[1] that the Kreisselmeier function (KF)

$$\mathrm{KF} = \frac{1}{\rho}\ln\sum_{j=1}^{k}\exp\left(\rho\frac{J_j}{c_j}\right) \tag{1}$$

be minimized. In this equation, $\rho > 0$ is a spread factor, J_j is the jth element of the vector performance index, c_j is the corresponding weighting factor, and k is the number of elements of the vector performance index. (In this example, $k = 8$.) This function approaches the original unconstrained minimization problem for sufficiently high values of ρ (Ref. 1).

The variation of the KF with respect to the time constants of $F(s)$ is shown in Fig. 2a. We note that $K(s)$ is first designed for the shaped plant for each set of the time constants $\tilde{\tau}_1$ and $\tilde{\tau}_2$ of $F(s)$, and the KF is subsequently computed. In Fig. 2a, the x, y, and z axes represent the zero location, the pole location, and KF for $\rho = 20$, respectively. Any higher value of ρ does not change the magnitude of KF.[3] We conclude from Fig. 2a that the minimum occurs when the pole $p = 0.05$. However, there are many values of the zero location that satisfy the minimum. A more careful tuning of the performance indices by setting permissible limits (for instance, setting a maximum permissible value of the peak overshoot at 10%) results in a value of $z = 2.0$. Consequently, these values are chosen as the pole and zero location of $F(s)$. Because $\tilde{\tau}_1 < \tilde{\tau}_2$, the compensator is obviously a lag network in the frequency range of interest. We note that unlike classical controller designs, where a lag compensator is added to improve the steady-state response, the feedback controller $K(s)$ in the present case is designed for the shaped plant. Thus, the effect of the lag filter in both cases may not be the same.

The Bode plot of the unshaped plant model transfer function from θ to the actuator input is shown in Fig. 2b. It is observed that the crossover frequency of the magnitude plot is approximately 15 rad/s. Moreover, the magnitude of the transfer function at the first two bending modes is rather high. On the contrary, these values are reduced with the addition of $F(s)$. Consequently, the interactions of the flexural dynamics with the rigid-body dynamics are less. The $\mathcal{H}_\infty$ controller is designed for this shaped plant model. The following weighting transfer matrices are chosen after several iterations: $W_1(s) = w_1(s)I_{n_i}$ and $W_2(s) = w_2(s)I_{n_i}$ where $w_1(s) = 10/(10s+1)(5s+1)$, $w_2(s) = 0.01(0.01s+1)/0.0001s+1$, and n_i is the number of inputs to the given plant $P(s)$. This choice serves to provide a good rolloff in the high-frequency ranges. The order of the generalized plant is 15. We note that the designed $K(s)$ is a stable function. The Bode plot of the open-loop transfer function with the loop broken at the plant input is shown in Fig. 2c. The phase margin computed from this Bode plot is found to be 21.17. It is noted that $\phi'_{\mathrm{pg}_j} = \phi'_{\mathrm{rg}_j}$ if the position and rate gyros are collocated. Therefore, under this assumption, the rate input to the controller can be absorbed into its transfer matrix resulting in a single-input/single-output (SISO) system. The Bode plot of this function is shown in Fig. 2d. We observe two notches at frequencies that correspond to the natural frequencies of the flexible modes. It is noted that this phenomenon is observed only after converting the two-input/one-output controller to an equivalent SISO system.

The time-domain performance of the closed-loop system is evaluated by carrying out linear simulation studies. The closed-loop system is subjected to a step input of 1 deg at the θ_m channel of the d input (Fig. 1), and the response shown in Fig. 3. Evidently, the system tracks the step command, although tracking is not an explicit objective of the design. [We observe that with a zero r input (Fig. 1), the output $y_p(s)$ of the plant $P(s)$ is given by $-P(s)F(s)K(s)[I + P(s)F(s)K(s)]^{-1}d(s)$; thus, in the steady state, $y_p(t)$ goes to -1 in response to the positive step input at d.] An overshoot of approximately 10% is observed. Moreover, the rise time of this response curve is within acceptable limits, and the settling time is approximately 2 s. Further, the displacement of the flexible modes q_1 and q_2 are rather small. The displacement of the third mode q_3 is even smaller and is not shown. We note that the maximum rates of these modes, respectively, are of the order of 0.01, 0.002, and 0.0001 m/s.

The controller order is reduced from 15 to 7 using the Hankel norm approximation approach.[5] We note that only marginal changes in the robustness and the time-domain performance with the reduced-order controller is observed. Further, this reduced-order controller is observed[3] to perform satisfactorily when the natural frequencies and the local slopes of the mode shape functions at the sensor locations are perturbed by 20%. These results are not included for brevity.

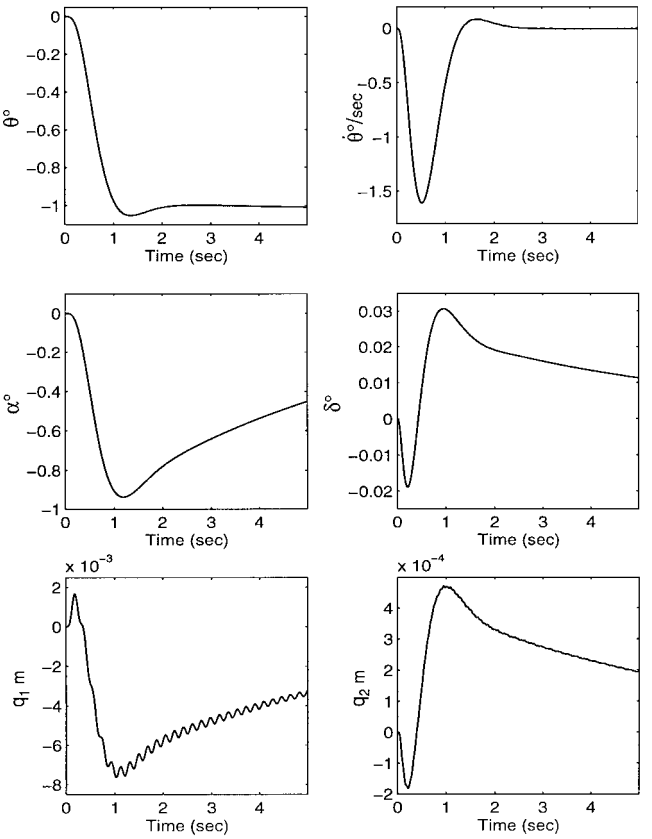

Fig. 3 Response to a step input of 1 deg at θ_m channel.

Conclusions

A novel method for the design of a two-DOF $\mathcal{H}_\infty$ robust controller is presented. The forward compensator is chosen to improve the time-domain performance; its parameters are obtained by a multicriteria optimization technique based on the minimization of the KF. An added advantage of the forward compensator is that the singular values of the plant are shaped a priori. The feedback compensator is then designed to make the closed-loop system robust. Thus, this method achieves time-domain performance as well as robustness. This method is then applied to design a robust controller for a flexible missile. It is observed that the two-DOF controller is open-loop stable, and that the closed-loop system has satisfactory robustness properties, as well as time-domain performance. Further, a reduced-order controller also yields the same robustness and time-domain performance.

References

[1] Kreisselmeier, G., and Steinhauser, R., "Systematic Control Design by Optimizing a Vector Performance Index," *Proceedings of the International Federation of Automatic Control Symposium on Computer Aided Design of Control Systems* (Zürich, Switzerland), Pergamon, Oxford, England, UK, 1980, pp. 113–117.

[2] Glover, K., and Doyle, J. C., "State-Space Formulae for all Stabilizing Controllers That Satisfy an $\mathcal{H}_\infty$ Norm Bound and Relations to Risk Sensitivity," *Systems and Control Letters*, Vol. 11, No. 3, 1988, pp. 167–172.

[3] George, K. K., "$\mathcal{H}_\infty$-Based Robust Controller for Aerospace Vehicles," Ph.D. Thesis, Dept. of Aerospace Engineering, Indian Inst. of Science, Bangalore, India, Nov. 1996.

[4] Horowitz, I. M., *Synthesis of Feedback Systems*, Academic, New York, 1963, Chap. 6.

[5] Safonov, M. G., and Chiang, R. Y., "A Schur Method for Balanced Model Reduction," *Proceedings of the 1988 American Control Conference* (Atlanta, GA), American Automatic Control Council, 1988, pp. 1036–1040.